THE PROTEIN SOCIETY

Disruption of the *E. coli* LptC dimerization interface and characterization of lipopolysaccharide and LptA binding to monomeric LptC

Kathryn M. Schultz, Matthew A. Fischer, Elizabeth L. Noey, and Candice S. Klug*

Department of Biophysics, Medical College of Wisconsin, Milwaukee, Wisconsin 53226

Received 9 January 2018; Accepted 17 April 2018
DOI: 10.1002/pro.3429
Published online 19 April 2018 proteinscience.org

Abstract: Lipopolysaccharide (LPS) is an essential element of nearly all Gram-negative bacterial outer membranes and serves to protect the cell from adverse environmental stresses. Seven members of the lipopolysaccharide transport (Lpt) protein family function together to transport LPS from the inner membrane (IM) to the outer leaflet of the outer membrane of bacteria such as *Escherichia coli*. Each of these proteins has a solved crystal structure, including LptC, which is a largely periplasmic protein that is associated with the IM $LptB_2FG$ complex and anchored to the membrane by an N-terminal helix. LptC directly binds LPS and is hypothesized to be involved in the transfer of LPS to another periplasmic protein, LptA. Purified and in solution, LptC forms a dimer. Here, point mutations designed to disrupt formation of the dimer are characterized using site-directed spin labeling double electron electron resonance (DEER) spectroscopy, light scattering, circular dichroism, and computational modeling. The computational studies reveal the molecular interactions that drive dimerization of LptC and elucidate how the disruptive mutations change this interaction, while the DEER and light scattering studies identify which mutants disrupt the dimer. And, using electron paramagnetic resonance spectroscopy and comparing the results to the previous quantitative characterization of the interactions between dimeric LptC and LPS and LptA, the functional consequences of monomeric LptC were also determined. These results indicate that disruption of the dimer does not affect LPS or LptA binding and that monomeric LptC binds LPS and LptA at levels similar to dimeric LptC.

Keywords: LptC; LPS; lipopolysaccharide; periplasmic protein; LPS binding protein; EPR spectroscopy; dimer; dissociation constant; electrostatic surface potential; computational modeling

Additional Supporting Information may be found in the online version of this article.

Statement of importance: The studies presented here use site-directed spin labeling EPR spectroscopy, computer modeling, and other complementary biophysical techniques to monitor the effects of mutations designed to disrupt LptC dimerization as well as characterize monomeric LptC for LPS and LptA binding capability. This work contributes to the understanding of the Gram-negative bacterial LPS transport machinery, an essential system with notable potential for antibiotic intervention.

Grant sponsor: National Institute of Biomedical Imaging and Bioengineering; Grant number: P41 EB001980; Grant sponsor: NIH Office of the Director; Grant number: S10 OD011937; Grant sponsor: National Institute of General Medical Sciences; Grant number: R01 GM108817; Grant sponsor: National Center for Research Resources; Grant numbers: S10 RR022422, S10 RR023748.

*Correspondence to: [Candice S. Klug, Department of Biophysics, Medical College of Wisconsin, 8701 Watertown Plank Road, Milwaukee, WI 53226]. E-mail: candice@mcw.edu

Introduction

The outer membranes (OM) of Gram-negative bacteria act as selective permeability barriers to vigilantly protect the cell from environmental stresses.[1] The outer leaflet of the OM is largely composed of lipopolysaccharide (LPS), an essential component of nearly all Gram-negative bacteria, and therefore, its synthesis and transport to the OM is critical to the survival of these bacteria. The Lpt (LPS transport) system of proteins[2–10] [Fig. 1(A)] is responsible for removing LPS from the outer leaflet of the inner membrane, transporting it across the periplasm, and inserting it into the outer leaflet of the OM. The structures of all seven proteins in the Lpt system involved in LPS transport in Gram-negative bacteria have now been solved[11–16] and provide helpful insights into the essential LPS transport process. For example, the soluble domain of LptC (amino acids 24–191) containing the point mutation G153R crystallized as a terminal dimer with the N-terminal β-strands forming the interaction interface[14] [Fig. 1(B)]. Our work using light scattering and double electron electron resonance (DEER) spectroscopy techniques confirmed this dimer conformation for the soluble WT LptC protein in vitro.[17] Our electron paramagnetic resonance (EPR) spectroscopy studies also used the application of pressure to monitor the stability of the LptC dimer at high pressure.[18] And, we investigated the stability of LptC upon addition of LptA to show that both the LptC protein conformation and the dimer are largely unaffected by binding to LptA.[17] In this work, we study the effects of six targeted mutations on the stability of the LptC dimer to understand if the dimer is required for function. Previous experiments from our lab introduced point mutations into LptA to disrupt oligomerization and monitored the resulting proteins with biophysical techniques.[19] Here, we took a similar strategy in the study of LptC.

While there is evidence for essential interactions with other proteins, such as LptA and $LptB_2FG$, in LPS transport, the functional relevance of the LptC homodimer in vivo is not understood. Therefore, we studied the effects of disruptive mutations on the N-terminal edge strand of LptC, the interface that interacts with itself in the dimer structure, using site-directed spin labeling (SDSL) EPR spectroscopy, light scattering, computational modeling, and circular dichroism (CD) spectroscopy techniques. A major strength of the EPR spectroscopy technique is the ability to detect and follow changes in local structure due to conformational changes or dynamic interactions with other proteins or substrates based on spin label mobility changes or distances between two spin labels.[20] This approach is ideally suited for the studies presented here on the structural and functional effects of disrupting the LptC dimer. In this work, we successfully created monomeric LptC proteins and then evaluated the functional implications of monomeric LptC upon binding to LPS and to LptA. Computational studies reveal the molecular interactions that drive dimerization and how the mutations affect this interface.

Results

Seven targeted point mutations and mutation combinations predicted to disrupt the N-terminal dimer interaction interface of LptC were introduced into LptC: Y60A, R61A, Y60A/R61A, Y60A/R61A/Y69A, A64R, V67R, and Y69A. The alanines were selected to remove large side chains possibly required for a stable interaction, and the arginines were selected to replace a large side chain or charge for small side chains to disrupt the interaction interface. Each of

Figure 1. Schematics of LptC. (A) Cartoon bridge model of the seven proteins involved in LPS transport. Multiple copies of LptA may span the periplasm, and LptE is located entirely inside of the barrel of LptD. The periplasmic domains of LptF and LptG, the soluble domain of LptC, LptA, and the periplasmic N-terminal domain of LptD all exhibit a similar β-jellyroll fold, likely enabling the formation of a stable bridge across the periplasm. (B) N-terminal dimer structure of LptC G153R as solved by crystallography (pdb: 4B54[14]). Terminal residues 24–57/58 and 183/184–191 are unresolved in the structure. (C) The two N-terminal edge strands from each protomer are shown with the studied residues shown in CPK format. Light green side chains are from one protomer and dark green side chains are from the other protomer. Black and gray residues are labeled and represent the mutation sites studied here.

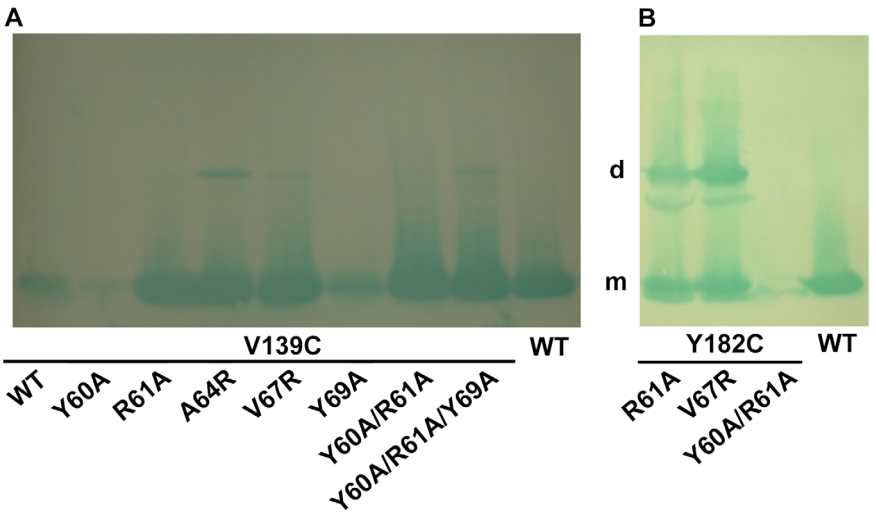

Figure 2. Western blots of whole BL21(DE3) cells expressing WT and LptC mutants, as indicated, from IPTG-inducible pET28b plasmids in the (A) V139C and (B) Y182C backgrounds. WT protein runs as a monomer (m). Disulfide-linked dimers (d) are also observed.

these mutations was introduced into LptC V139C, which when spin labeled acts as a dimerization reporter group, or LptC Y182C, which acts as an LPS and LptA binding reporter, for the EPR spectroscopy studies described below and then studied computationally.

Expression and protein folding of LptC N-terminal edge strand mutants

Each of the seven potentially disruptive LptC N-terminal mutations was first tested for expression in vivo. BL21(DE3) cells were transformed with plasmid encoding for an inducible 6xHis-tagged soluble mutant LptC protein, and whole cells were assessed for IPTG-induced LptC expression by SDS–PAGE and Western blot. The data in Figure 2(A) show that five of the mutated proteins in the V139C background is expressed at levels similar to WT LptC; LptC V139C, V139C/Y60A, and V139C/Y69A are expressed at levels less than WT.

Each of the overexpressed LptC mutant proteins was then purified from the soluble fraction of *E. coli* using affinity chromatography. Cells expressing LptC V139C/A64R did not yield purified protein. The six remaining proteins were successfully purified, spin labeled at V139C with a sulfhydryl-specific spin label to generate the R1 side chain (see Methods), and then analyzed for secondary structure by CD spectroscopy. WT LptC exhibits a CD spectrum indicative of predominantly β-sheet structure (Fig. 3), in agreement with previous CD data collected on LptC.[17] LptC mutants V139R1, V139R1/R61A, and V139C/Y69A exhibit CD spectra that overlay well with the WT spectrum. LptC mutants V139R1/Y60A, V139R1/Y60A/R61A, V139R1/Y60A/R61A/Y69A, and V139R1/V67R show a largely similar but slightly altered spectral line shape indicating that the predominant β-sheet structure remains intact with the possible conversion to a slightly increased random coil content as exhibited by the decreased dichroism in the 190–210 nm region (Fig. 3). The CD data indicate that these mutations have minimal effect on the overall structure of the protomer.

Detecting disruption of the LptC dimer

Next, we tested the effect of the mutations on the ability of LptC to dimerize. LptC V139R1 was shown previously to be an excellent reporter of LptC dimerization using DEER spectroscopy,[17] and therefore was used here in the same manner.

Using DEER spectroscopy, the extent of dimerization of different protein samples can be directly compared. The modulation depth of the background-corrected dipolar evolution data collected using DEER spectroscopy can be a quantitative indicator of the number of spins involved in dimerization,[21,22] provided a number of experimental factors remain constant between samples, thus allowing the determination of the extent of dimerization of different potentially disruptive LptC mutants. We observe a distance distribution between the V139R1 sites on each protomer due to the dimerization of LptC. The separated peaks at 20 Å and 25 Å within the overall distribution are likely due to rotameric preferences, as suggested by the MMM predicted distance distribution (see gray area plots in Fig. 4). It is expected that each V139R1 is involved in a dimeric interaction at 100 μM as light scattering studies indicated that LptC forms a stable, concentration-independent dimer even at low (1 μM) concentrations.[17]

The six purified LptC mutants, each in combination with V139R1, were analyzed by DEER spectroscopy (Fig. 4). The point mutations R61A and Y69A had no effect on the population of LptC proteins involved

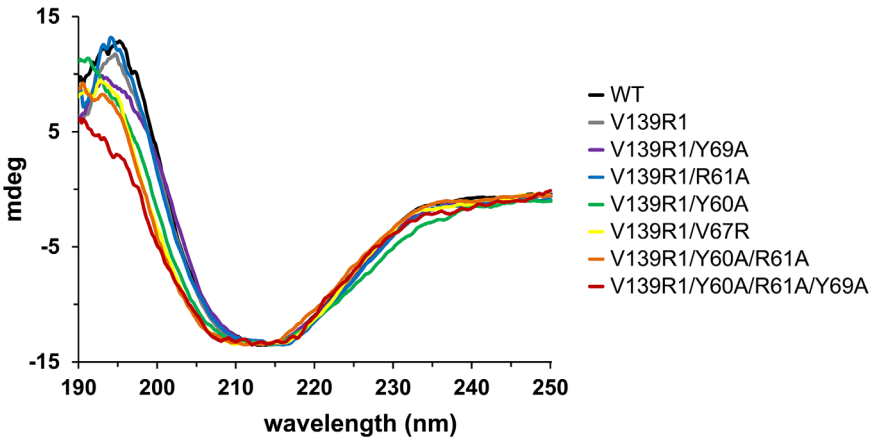

Figure 3. Far UV CD spectra of purified LptC protein, as indicated, scaled to align with the WT LptC data.

in dimerization nor on the dimer orientation; the modulation depth of the dipolar evolution data and the distance distributions remained similar to WT LptC. Y60A, Y60A/R61A, Y60A/R61A/Y69A, and V67R almost completely disrupted dimerization as indicated by the large reductions in the modulation depths and the resulting loss of the 20 and 25 Å peaks in the distance distributions (Fig. 4). Clearly, these mutations are disruptive to the dimer interface and result in monomeric LptC in solution. The effect of ionic strength on dimer formation was also tested. Raising the ionic strength from 240 m*M* NaCl to 1000 m*M* NaCl did not disrupt LptC dimer formation; decreasing the ionic strength of the buffer to 0 m*M* NaCl did not result in the formation of LptC V67R N-terminal dimers (Fig. S1).

In a complementary experiment, the oligomerization state was also analyzed using size-exclusion

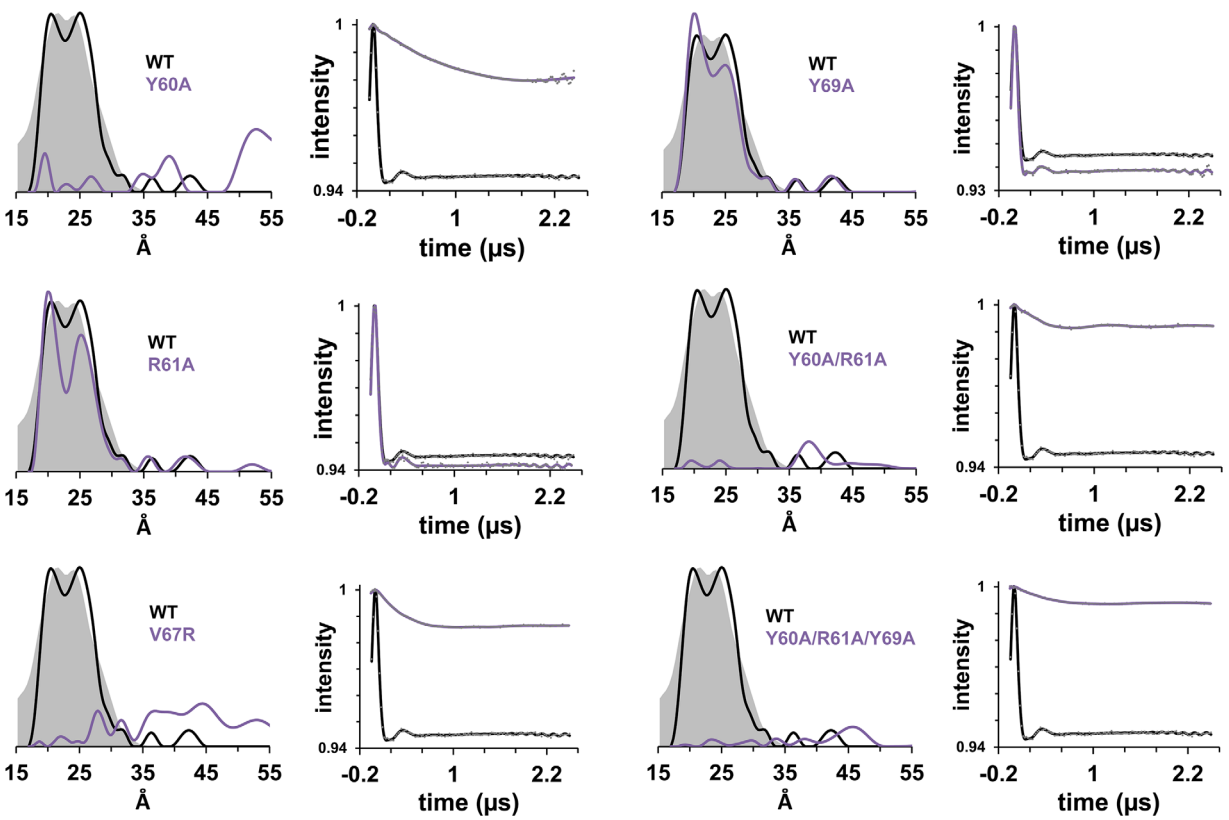

Figure 4. Q-band DEER spectroscopy data(Left) The experimentally derived distance distribution data are shown as solid lines and the predicted distribution for V139R1 calculated by MMM using the dimeric crystal structure of LptC (pdb:4B54) as gray area plots. The y-axes represent the distance probability and the data within each plot are scaled according to the modulation depth of the dipolar evolution data. (Right) Background-corrected dipolar evolution data (gray dots) and fits (solid lines) for 100 µ*M* LptC V139R1 samples in the WT (black lines) or mutant (purple lines) background as indicated.

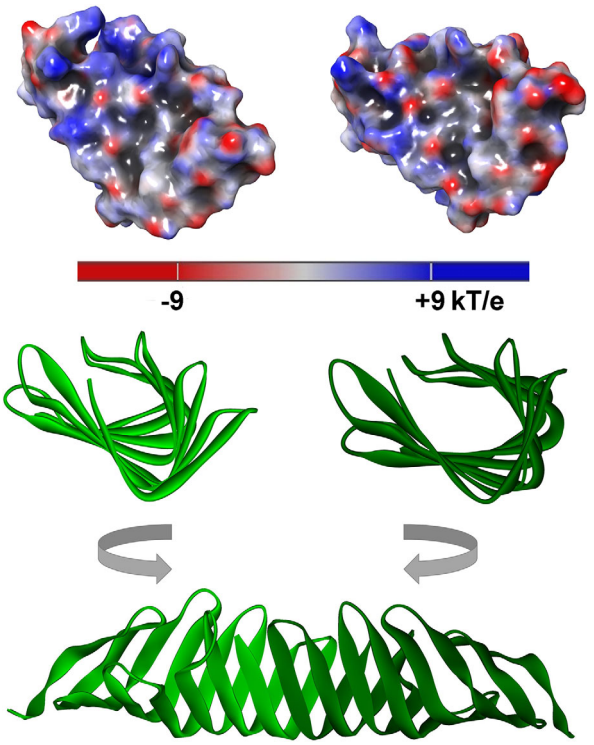

Figure 5. Poisson-Boltzmann electrostatic potential surfaces[32,33] calculated for the LptC crystal structure (pdb: 4B54[14]) chain B (left) and chain A (right) showing the N-terminal edge strands face on. Red represents negatively charged surfaces and blue represents positively charged surfaces. The dimer interface is formed by rotating the structures 90° toward each other such that the oppositely charged surfaces interact.

chromatography laser light scattering (SEC-LS), which gives the weight-average molecular weight (MW) of proteins in solution. At 1 μ*M* and 42 μ*M*, the major elution peak of soluble LptC V139C/Y60A/R61A had an average molecular weight of 20.4 kDa ± 5% and 22.8 kDa ± 5%, respectively. These data closely match the 21.2 kDa molecular weight of the 6x-His-tagged mutant LptC protomer, supporting the DEER data presented above that show that this mutant is monomeric in solution. In contrast, WT LptC previously exhibited an average molecular weight of 43.7 kDa ± 5%, which is twice that of the monomer.[17]

The LptC dimer was next studied computationally to investigate the molecular interactions that drive dimerization and how the disruptive mutations change this interaction. First, the electrostatic potential surface of the N-terminal edge strand of LptC, which forms the dimer interface, was mapped (Fig. 5). The color coding shows one side of the edge strand is more negatively charged (red) and the other side is more positively charged (blue). These results show that formation of the dimer interface using these edge strands is driven by complementary electrostatics, where the red region on the right side of the N-terminal edge strand interfaces with the blue region on the left side of the N-terminal edge strand.

The WT LptC dimer interface was further examined with all-atom molecular dynamics (MD) simulation. This simulation allowed relaxation of the side chains and secondary structure; an overlay of the snapshots from the simulation shows the conformational flexibility of the dimer and mutated side chains (Fig. 6). The structural fluctuations over time reveal that the β-strands are highly maintained throughout the simulation (Fig. S2), as expected. Interactions between the side chains of the two N-terminal edge strands of the protomers within the WT LptC dimer were analyzed over the course of the simulation, and on average, 16 H-bond contacts are maintained between chains, 8.6 involving the backbone atoms and 7.4 involving side chains (Table S1). The MD simulation revealed that Y60 and Y69 maintain 1 and 2 H-bonds, respectively, to the adjacent chain through backbone interactions. R61, on the other hand, maintains on average 1.8 H-bonds with the adjacent chain completely via the side-chain. Depending on its orientation, R61 forms a salt bridge with D72 or E68 (Fig. S3).

The effect of the mutations was analyzed by modeling them onto the crystal structure of dimeric LptC (pdb: 4B54). Figure 7 shows the LptC protomer with the N-terminal interaction interface residue change upon mutation highlighted for the seven mutants tested. Two single mutations do not disrupt the dimerization of LptC; the R61A mutation removes a large positively charged arginine from the surface of the protein and replaces it with a small hydrophobic alanine [Fig. 7(A)]. This mutation eliminates the salt bridges and H-bond contacts observed in the MD simulation but does not disrupt dimerization. The Y69A mutation replaces a large hydrophobic tyrosine residue with a small hydrophobic alanine, which eliminates hydrophobic contacts within the same protomer as well as between chains, but no H-bond contacts are lost between protomers, resulting in a protein still able to form a stable dimer interface.

The single mutant Y60A eliminates hydrophobic contacts similar to Y69A, yet this tyrosine to alanine substitution results in the inability to form a stable interaction interface. Not surprisingly, the double and triple alanine mutants Y60A/R61A and Y60A/R61A/Y69A [Fig. 7(D)] have similar effects as the single Y60A mutation. The combination mutants appear to change the properties of the interface without introducing major clashes to the structure. The single V67R mutation [Fig. 7(C)] also disrupted dimerization. The arginine substitution for valine eliminates favorable hydrophobic interactions between the two protomers within the dimer and the arginine points out into the solvent, which is

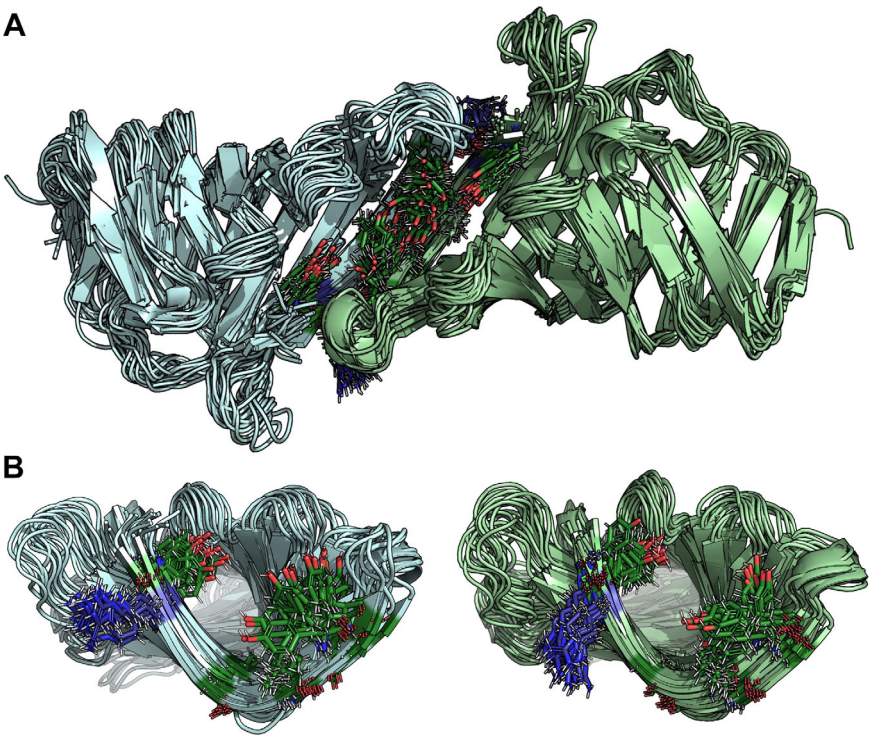

Figure 6. Overlay of snapshots from the WT LptC dimer MD simulation showing (A) the dimer and (B) each protomer with the N-terminal edge shown face on. The residues shown as sticks were mutated in this work. Chains B and A are pale cyan and pale green, respectively, with hydrophobic residues Y60, A64, V67, and Y69 colored green and R61 colored blue. Red indicates oxygen atoms and gray indicates hydrogen atoms.

incompatible with dimerization as the positively charged residue would then need to be accommodated by the already crowded hydrophobic core of the interacting protomer upon dimerization. As shown experimentally, the V67R mutation does not support dimerization of LptC.

The A64R mutation replaces a small hydrophobic alanine [Fig. 7(B)] in the crowded hydrophobic core of LptC with a large positively charged arginine residue. This mutation likely cannot be accommodated within the protein core due to its size and charge while maintaining the fold and conformation seen in the WT protein. This information, coupled with the experimental data showing that protein containing the A64R mutation is unable to be purified from the soluble fraction of the cell, suggests that the arginine substitution is disruptive to protein stability in vivo.

In summary, the single point mutations Y60A and V67R and the combination mutants Y60A/R61A and Y60A/R61A/Y69A prevent the dimerization of LptC but do not disrupt the overall protein fold, while the A64R mutation is disruptive to the overall protein stability.

Does monomeric LptC bind LPS?

The single point mutant V67R that results in a folded, monomeric LptC protein was then used to test the effect of oligomerization on LptC binding to LPS by EPR spectroscopy. For these studies, Y182R1 was selected because it was previously shown to be an excellent reporter of LPS binding by EPR spectroscopy and because it is conveniently located on the C-terminal edge of the protein, which is on the opposite end of the protein as the dimer interface being disrupted. Characterization of the Y182R1 mutant previously generated a dissociation constant of 11 μM for the WT LptC–LPS interaction and an LptC:LPS binding ratio of 1:1 for the dimeric LptC–LPS interaction.[17]

In these studies, LptC mutant Y182R1/V67R was used to test the binding of LPS to monomeric LptC. Interestingly, the Y182R1/Y60A/R61A mutant combination does not purify from the soluble fraction, so this mutant was unable to be analyzed for LPS binding [Fig. 2(B)]. Analysis of the EPR spectra of LptC Y182R1/V67R in the presence of increasing concentrations of LPS (Fig. 8) reveals a Kd of 12 μM for the monomeric LptC–LPS interaction (Fig. 9). 97% of the Y182R1/V67R proteins were affected by LPS binding in the presence of 198 μM LPS. The monomeric protein still bound one LPS per protomer, based on its B_{max} value of 103%. These values are remarkably similar to those determined for dimeric LptC, clearly indicating that disruption of the dimer does not affect LPS binding and that monomeric LptC does bind LPS at levels similar to dimeric LptC.

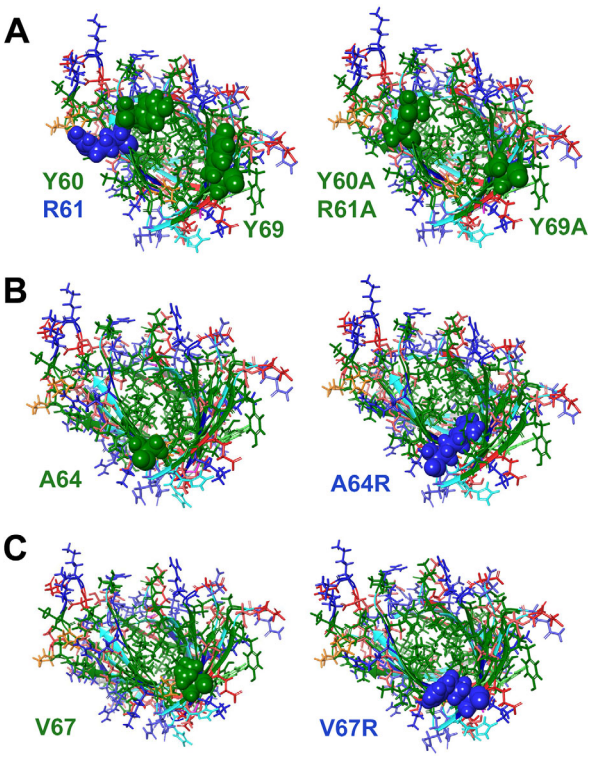

Figure 7. N-terminal edges of WT (left) and mutant (right) LptC protomer models based on the crystal structure (pdb:4B54[14]). Mutation site residues examined are shown in CPK as indicated. All other residues in the structure are represented by sticks and colored by type where hydrophobic residues A, V, I, L, F, and Y are green; positively charged residues R and K are blue, and H is light blue; negatively charged D and E are red; hydroxyl side chains S and T are salmon; and amide side chains N and Q are purple, G is magenta, and P is orange.

Does monomeric LptC bind LptA?

Monomeric LptC was tested for the ability to bind to LptA. Given the location of the LptA:LptC binding interface on the C-terminal edge of LptC, the ability to dimerize is not expected to interfere with its ability to bind to LptA. Nonetheless, this hypothesis was tested using EPR spectroscopy and Y182R1 as the reporter group. Y182R1 was also previously identified as an excellent reporter for the LptA–LptC interaction.[19] This spin label has relatively unrestricted motion in the absence of LptA or LPS, given its location on the C-terminal edge strand. Upon addition of LptA, the spin label motion on Y182R1 in the A67R background becomes highly restricted [Fig. 8(B)], as it does in the WT background.[19] Analysis of LptC Y182R1/V67R spectra in the presence of increasing concentrations of WT LptA revealed a K_d of 1 μM and a B_{max} value of 85% for the monomeric LptC–WT LptA interaction (Fig. 9). Compared with a K_d of 4 μ*M* and a B_{max} of 83% for the WT LptC–WT LptA interaction,[19] these data indicate that LptC monomers bind LptA with similar affinity as LptC dimers. Thus, monomerization of LptC does not adversely affect the LptC–LptA interaction.

Discussion

Two of the N-terminal single mutations tested to disrupt LptC dimer formation successfully resulted in a predominantly monomeric population of proteins. LptC single mutants Y60A and V67R and the combination Y60A/R61A and Y60A/R61A/Y69A mutants each resulted in a protein that was unable to form dimers. Of note, R61A and Y69A alone do not disrupt dimerization, so the results of the combination mutants containing Y60A are solely due to the destabilizing effects of Y60A. Raising the ionic strength of the buffer does not affect dimerization and decreasing ionic strength does not undo the disruptive effects of the V67R mutation (Fig. S3). Based on the modulation depth of the dipolar evolution data for V67R in the absence of salt, the complete removal of salt from the buffer may induce a small population of the LptC proteins to oligomerize in another configuration. These data suggest that electrostatics alone are not enough to drive N–N dimerization. Computations on the effects of the two point mutations experimentally shown here to disrupt dimerization show that hydrophobic interactions appear to largely drive the interaction.

We previously used the application of pressure, in lieu of mutations, to disrupt the LptC dimer.[18] In that work, LptC was shown to unfold at its C-terminal edge strand, yet the core and N-terminal edge of the soluble fraction of the protein adopted an alternate, likely monomeric, conformational state upon application of high hydrostatic pressure. Quantitative evaluation of DEER data obtained using LptC S95R1 revealed that the distance distribution resulting from these reporter sites was largely unchanged when comparing the 0 and 2 kbar data for LptC S95R1; however, the modulation depths of the dipolar evolution data indicated that approximately half of the dimers were likely monomeric at 2 kbar of pressure.[18]

The overall distance distributions between V139R1 containing Y60A or V67R suggest that there may be a small population of proteins with distances between V139R1 sites that are longer than the distances observed between the WT N–N dimer. In addition, a small population of distances representing the N–N dimer remain at 100 μ*M* protein concentration for these proteins. The light scattering data for the LptC V139C/Y60A/R61A protein at 1 μ*M* indicate that the average mass of the protein (20.4 kDa) is the same as expected for the monomer (21.2 kDa) within the 5% error of the technique (19.4–21.4 kDa). However, at 42 μM, the average mass range of 21.7–23.9 kDa (22.8 ± 5% kDa) is slightly higher than the 21.2 kDa mass expected for

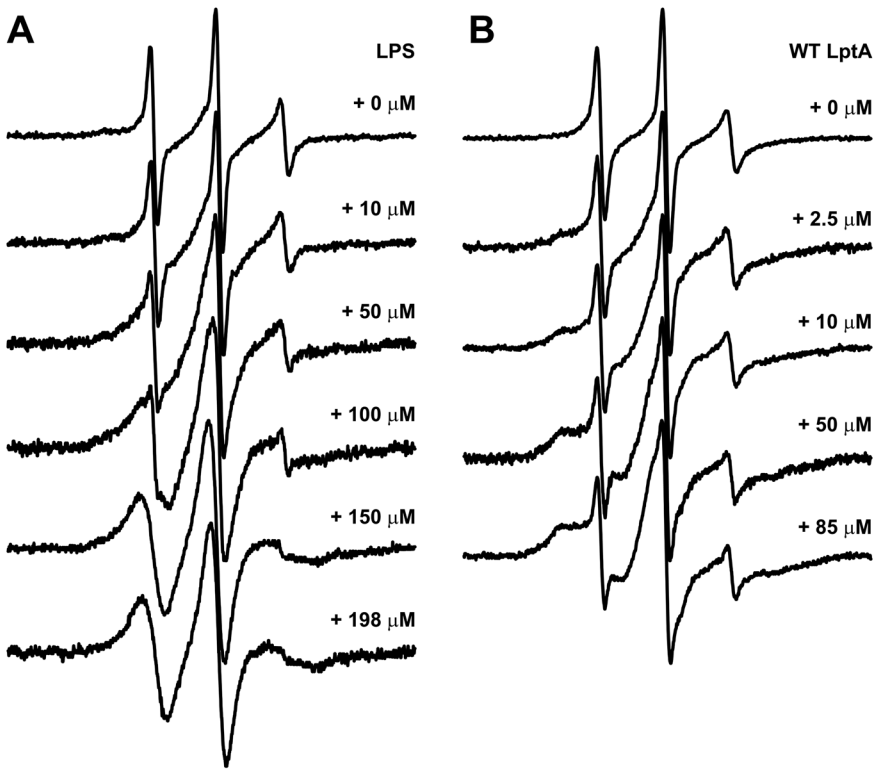

Figure 8. X-band CW EPR spectra (100 G) for the LptC Y182R1/V67R protein at (A) 2 μ*M* in the presence of LPS and at (B) 10 μ*M* in the presence of WT LptA.

the monomer, which may suggest that there is a small percentage of dimers of some orientation remaining, and is consistent with the DEER data collected at higher concentrations.

In vivo expression of the LptC V139C mutants does not appear to correlate with ability to dimerize. While V139C/Y60A expresses at a low level and disrupts dimerization, V139C and V139C/Y69A also express at low levels but do not disrupt dimerization. Further, the disruptive V139C/V67R, V139C/Y60A/R61A and V139C/Y60A/R61A/Y69A LptC mutants express at WT levels. And, protein containing the V139C/Y60A/R61A mutation combination has robust expression and is readily purified, yet the Y182C/Y60A/R61A mutant does not express. V139C is located on a loop and Y182C is located on the C-terminal edge strand, both in locations that were not expected to interfere with dimer formation. Furthermore, the Y182C mutation has been introduced into an array of other background mutations with no adverse effects on protein expression or stability and has been used in the WT background as a reporter to successfully quantitate LPS and LptA binding to LptC. It is possible that this combination is unstable or misfolds; however, it is yet unclear specifically why the combination of these three specific mutations has a detrimental

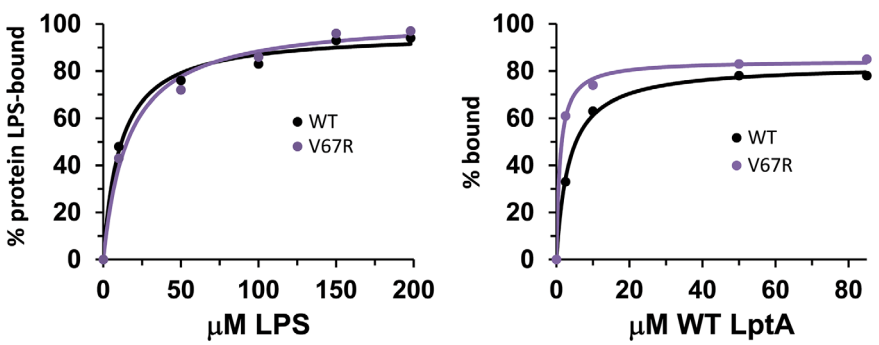

Figure 9. Data plots and fits to determine K_d and B_{max} values for LptC Y182R1/V67R binding to LPS (left) and WT LptA (right). Resulting data (circles) from the deconvolution of the composite EPR spectra shown in Figure 8 are plotted against ligand concentration and fit to a single site binding model (solid lines). The resulting K_d values are 12 ± 1 μ*M* and 1 ± 0 μ*M*, and B_{max} values are $103 \pm 2\%$ and $85 \pm 1\%$, for the monomeric LptC–LPS and LptC–LptA interactions, respectively.

effect on expression. In contrast, LptC mutants Y182C/R61A and Y182C/V67R are both readily expressed [Fig. 2(A)].

Conclusions

LptC dimerization can be inhibited by point mutations along the interface that remove critical hydrophobic interactions. Monomeric LptC retains its ability to bind LPS and LptA at WT levels, suggesting that its function is not related to dimerization. Our data support the hypothesis that LptC may be monomeric in vivo.[18] If the dimer is not required to bind to LPS or to LptA, it may be that the dimer is not functionally necessary. In solution, in the absence of LptF or LptG, it is possible that the N-terminal edge strand of LptC may interact with itself for lack of a relevant binding partner.

Materials and Methods

Site-directed mutagenesis

Mutations were introduced into the gene of the LptC soluble domain (amino acids 24–191) using High Fidelity PCR EcoDry Premix (Clontech, Mountain View, CA) and sequencing at Retrogen (San Diego, CA) or by commercial gene synthesis or site-directed mutagenesis (GenScript, Piscataway, NJ).[19,23]

Protein expression and purification

LptC mutants encoded within a pET28b (Novagen, EMD Millipore, Billerica, MA) vector with an N-terminal 6xHis tag were expressed using IPTG in *E. coli* BL21(DE3) cells.[19,23] Whole cells were pelleted, boiled, subjected to 12% SDS-PAGE (Biorad, Hercules, CA), transferred to PVDF membranes, and analyzed by Western blot using the Penta-His antibody against the His-tag (Qiagen, Germantown, MD) to qualitatively compare the overall levels of protein expression in vivo.

LptC mutants were purified from the soluble fraction by cobalt affinity chromatography (Clontech, Mountain View, CA), the R1 side chain was generated by the addition of the sulfhydryl-specific 2,2,5,5-tetramethylpyrroline-3-yl-methanethiosulfonate spin label (MTSL; Toronto Research Chemicals, New York, ON) to the introduced cysteine residue, and proteins were concentrated as described previously.[19,23] LPS from *E. coli* O111:B4 (List Biological Laboratories, Inc., Campbell, CA) was resuspended at 200 μ*M* in the same buffer used for purified LptC protein (50 m*M* $NaPO_4$, 300 m*M* NaCl, pH 7.0).

CD spectroscopy

Purified LptC proteins were dialyzed to remove salt and imidazole, and the final protein concentration in each sample was 5 μ*M* in 50 m*M* $NaPO_4$, pH 7.0 buffer. The CD spectra were recorded at room temperature on a Jasco J-710 spectropolarimeter in a 0.1 cm pathlength cuvette using a 0.2 nm resolution step, a 0.5 s time constant, and signal averaged 10 times.

Light scattering

Purified LptC V139C/Y60A/R61A protein was analyzed by multi-angle SEC-LS at the Keck Biotechnology Resource Laboratory at Yale University,[24,25] as described previously for analysis of WT LptC.[17] Briefly, the purified protein was filtered, passed through a size exclusion column, detected by a DAWN-EOS light detector (Wyatt Technologies, Santa Barbara, CA), and analyzed using ASTRA (Wyatt Technologies, Santa Barbara, CA).

EPR spectroscopy data collection and analysis

Continuous wave (CW) EPR spectroscopy data were collected using a Bruker E500 (Bruker BioSpin Corporation, Billerica, MA) with a Bruker ER4122 SHQE-W1 cavity, a 42 s scan time, and a 1.5 G modulation amplitude under nonsaturating power at room temperature. The low concentration (2 μ*M*) protein samples were contained in AquaStar tubing developed at the National Biomedical EPR Center.[26]

DEER spectroscopy data were collected on a Bruker Q-band E580 spectrometer using an overcoupled Bruker EN5107D2 resonator. EPR samples containing 20% deuterated glycerol as a cryoprotectant were flash frozen in a dry ice and acetone mixture and run at 80 K. The resulting data were phased and background corrected using the LongDistances software program (http://www.biochemistry.ucla.edu/biochem/Faculty/Hubbell/)[27] written by C. Altenbach (University of California-Los Angeles, CA). The experimental distance distributions resulted from fits to the background-corrected dipolar evolution data using the model-free algorithms in the LongDistances program. The x-axes of the distance distribution plots in Figure 4 indicate the reliable distance limits for the data presented,[28] and the predicted distance distributions were determined using MMM 2013.2.[29]

The CW spectra were analyzed using spectral subtraction to determine the percent of protein affected by LPS or LptA binding as described previously.[17] Briefly, the multiple component spectra recorded in the presence of LPS were manually deconvoluted to obtain the respective LPS-bound spectra through spectral subtraction of the corresponding apo spectrum, and the number of spins affected by the presence of LPS or LptA were divided by the total number of spins in each composite spectrum.

Computational modeling

The LptC crystal structure (pdb: 4B54[14]) with G153R mutated back to WT (i.e., G153) was the starting point for all computational modeling. The structure was prepared with Schrodinger's Protein Preparation tool, where hydrogens were added to

the structure and H-bonds were minimized.[30,31] The Poisson-Boltzmann electrostatic potential surface[32,33] of each protomer was created in Maestro with implicit solvent and scaled −9 to +9 kT/e. Point mutations were modeled onto the WT structure, and the rotamers were chosen based on minimizing steric interactions with existing side chains.

All-atom MD simulations of the WT LptC dimer were run with Desmond,[34] using a tip3p water box of size 110 $Å^3$ with 50 m*M* NaCl. The system was minimized and equilibrated with Schrodinger's standard protocol. The simulation was run at 300 K for 500 ns and snapshots were recorded every 1.2 ns. Analysis was executed with Schrodinger's MD analysis tools Simulation Interaction Diagram and Simulation Event Analysis.[35]

Supplementary Material

Additional data are presented in the Supplementary materials file (Disruption of LptC dimer_Supplementary Material.pdf).

Acknowledgments

The authors thank Jimmy Feix for critical reading of the manuscript. This work was supported by National Institute of Health grants R01 GM108817, P41 EB001980 (National Biomedical EPR Center), S10 RR022422 and S10 OD011937 (DEER instrumentation), and S10 RR023748 (Keck Biotechnology Resource Laboratory SEC-LS/UV/RI instrumentation at Yale University).

References

1. Nikaido H (2003) Molecular basis of bacterial outer membrane permeability revisited. Microbiol Mol Biol Rev 67:593–656.
2. Bos MP, Tefsen B, Geurtsen J, Tommassen J (2004) Identification of an outer membrane protein required for the transport of lipopolysaccharide to the bacterial cell surface. Proc Natl Acad Sci U S A 101:9417–9422.
3. Wu T, McCandlish AC, Gronenberg LS, Chng SS, Silhavy TJ, Kahne D (2006) Identification of a protein complex that assembles lipopolysaccharide in the outer membrane of *Escherichia coli*. Proc Natl Acad Sci U S A 103:11754–11759.
4. Sperandeo P, Cescutti R, Villa R, Di Benedetto C, Candia D, Deho G, Polissi A (2007) Characterization of lptA and lptB, two essential genes implicated in lipopolysaccharide transport to the outer membrane of *Escherichia coli*. J. Bacteriol 189:244–253.
5. Ruiz N, Gronenberg LS, Kahne D, Silhavy TJ (2008) Identification of two inner-membrane proteins required for the transport of lipopolysaccharide to the outer membrane of *Escherichia coli*. Proc Natl Acad Sci U S A 105:5537–5542.
6. Sperandeo P, Lau FK, Carpentieri A, De Castro C, Molinaro A, Deho G, Silhavy TJ, Polissi A (2008) Functional analysis of the protein machinery required for transport of lipopolysaccharide to the outer membrane of *Escherichia coli*. J. Bacteriol 190:4460–4469.
7. Narita S, Tokuda H (2009) Biochemical characterization of an ABC transporter LptBFGC complex required for the outer membrane sorting of lipopolysaccharides. FEBS Lett 583:2160–2164.
8. Ruiz N, Kahne D, Silhavy TJ (2009) Transport of lipopolysaccharide across the cell envelope: the long road of discovery. Nat Rev Microbiol 7:677–683.
9. Chng SS, Ruiz N, Chimalakonda G, Silhavy TJ, Kahne D (2010) Characterization of the two-protein complex in *Escherichia coli* responsible for lipopolysaccharide assembly at the outer membrane. Proc Natl Acad Sci U S A 107:5363–5368.
10. Freinkman E, Chng SS, Kahne D (2011) The complex that inserts lipopolysaccharide into the bacterial outer membrane forms a two-protein plug-and-barrel. Proc Natl Acad Sci U S A 108:2486–2491.
11. Zhou Z, White KA, Polissi A, Georgopoulos C, Raetz CR (1998) Function of *Escherichia coli* MsbA, an essential ABC family transporter, in lipid A and phospholipid biosynthesis. J Biol Chem 273:12466–12475.
12. Suits MD, Sperandeo P, Deho G, Polissi A, Jia Z (2008) Novel structure of the conserved gram-negative lipopolysaccharide transport protein A and mutagenesis analysis. J Mol Biol 380:476–488.
13. Tran AX, Dong C, Whitfield C (2010) Structure and functional analysis of LptC, a conserved membrane protein involved in the lipopolysaccharide export pathway in *Escherichia coli*. J Biol Chem 285:33529–33539.
14. Villa R, Martorana AM, Okuda S, Gourlay LJ, Nardini M, Sperandeo P, Deho G, Bolognesi M, Kahne D, Polissi A (2013) The *Escherichia coli* Lpt transenvelope protein complex for lipopolysaccharide export is assembled via conserved structurally homologous domains. J Bacteriol 195:1100–1108.
15. Dong H, Xiang Q, Gu Y, Wang Z, Paterson NG, Stansfeld PJ, He C, Zhang Y, Wang W, Dong C (2014) Structural basis for outer membrane lipopolysaccharide insertion. Nature 511:52–56.
16. Qiao S, Luo Q, Zhao Y, Zhang XC, Huang Y (2014) Structural basis for lipopolysaccharide insertion in the bacterial outer membrane. Nature 511:108–111.
17. Schultz KM, Klug CS (2018) Characterization of and lipopolysaccharide binding to the *E. coli* LptC protein dimer. Protein Sci 27:381–389.
18. Schultz KM, Klug CS (2017) High-pressure EPR spectroscopy studies of the *E. coli* lipopolysaccharide transport proteins LptA and LptC. Appl Magn Reson 48: 1341–1353.
19. Schultz KM, Feix JB, Klug CS (2013) Disruption of LptA oligomerization and affinity of the LptA-LptC interaction. Protein Sci 22:1639–1645.
20. Klug CS, Feix JB. Methods and applications of site-directed spin labeling EPR spectroscopy. In: Correia JJ, Detrich HW, Eds. (2008) Biophysical tools for biologists, Vol. 1: in vitro techniques. Oxford, UK: Academic Press, pp 617–658.
21. Bode BE, Margraf D, Plackmeyer J, Durner G, Prisner TF, Schiemann O (2007) Counting the monomers in nanometer-sized oligomers by pulsed electron-electron double resonance. J Am Chem Soc 129:6736–6745.
22. Hilger D, Jung H, Padan E, Wegener C, Vogel KP, Steinhoff HJ, Jeschke G (2005) Assessing oligomerization of membrane proteins by four-pulse DEER: pH-dependent dimerization of NhaA Na+/H+ antiporter of *E. coli*. Biophys J 89:1328–1338.
23. Merten JA, Schultz KM, Klug CS (2012) Concentration-dependent oligomerization and oligomeric arrangement of LptA. Protein Sci 21:211–218.
24. Folta-Stogniew E (2006) Oligomeric states of proteins determined by size-exclusion chromatography coupled

with light scattering, absorbance, and refractive index detectors. Methods Mol Biol 328:97–112.
25. Folta-Stogniew E, Williams KR (1999) Determination of molecular masses of proteins in solution: implementation of an HPLC size exclusion chromatography and laser light scattering service in a core laboratory. J Biomol Tech 10:51–63.
26. Sidabras JW, Mett RR, Hyde JS (2017) Extruded dielectric sample tubes of complex cross section for EPR signal enhancement of aqueous samples. J Magn Reson 277:45–51.
27. Toledo Warshaviak D, Khramtsov VV, Cascio D, Altenbach C, Hubbell WL (2013) Structure and dynamics of an imidazoline nitroxide side chain with strongly hindered internal motion in proteins. J Magn Reson 232:53–61.
28. Jeschke G (2012) DEER distance measurements on proteins. Annu Rev Phys Chem 63:419–446.
29. Polyhach Y, Bordignon E, Jeschke G (2011) Rotamer libraries of spin labelled cysteines for protein studies. Phys Chem Chem Phys 13:2356–2366.
30. Sastry GM, Adzhigirey M, Day T, Annabhimoju R, Sherman W (2013) Protein and ligand preparation: parameters, protocols, and influence on virtual screening enrichments. J Comput Aided Mol Des 27:221–234.
31. Schrödinger Release 2017-4: Schrödinger Suite 2017-4 Protein Preparation Wizard; Epik, Schrödinger, LLC, New York, NY, 2016; Impact, Schrödinger, LLC, New York, NY, 2016; Prime, Schrödinger, LLC, New York, NY, 2017.
32. Gouy M (1910) Sur la constitution de la charge électrique à la surface d'un électrolyte. J Phys Theor Appl 9:457–468.
33. Chapman DL (1913) A contribution to the theory of electrocapillarity. Philos Mag 25:475–481.
34. Schrödinger Release 2017-4: Desmond molecular dynamics system. New York: D. E. Shaw Research2017; Schrödinger, New York: Maestro-Desmond Interoperability Tools, 2017.
35. Guo Z, Mohanty U, Noehre J, Sawyer TK, Sherman W, Krilov G (2010) Probing the alpha-helical structural stability of stapled p53 peptides: molecular dynamics simulations and analysis. Chem Biol Drug Des 75:348–359.
36. Hatmal MM, Li Y, Hegde BG, Hegde PB, Jao CC, Langen R, Haworth IS (2012) Computer modeling of nitroxide spin labels on proteins. Biopolymers 97:35–44.